Published in final edited form as:
Nature. 2009 March 12; 458(7235): 233–237. doi:10.1038/nature07642.

Coenzyme recognition and gene regulation by a flavin mononucleotide riboswitch

Alexander Serganov[*], **Lili Huang**[*], and **Dinshaw J. Patel**
Structural Biology Program, Memorial Sloan-Kettering Cancer Center, New York, NY, 10065

Abstract

The biosynthesis of several protein cofactors is subject to feedback regulation by riboswitches[1–3]. Flavin mononucleotide (FMN)-specific riboswitches[4,5], also known as RFN elements[6], direct expression of bacterial genes involved in the biosynthesis and transport of riboflavin (vitamin B_2) and related compounds. Here we present the crystal structures of the *Fusobacterium nucleatum* riboswitch bound to FMN, riboflavin and antibiotic roseoflavin[7]. The FMN riboswitch structure, centred on an FMN-bound six-stem junction, does not fold by collinear stacking of adjacent helices, typical for folding of large RNAs. Rather, it adopts a butterfly-like scaffold, stapled together by opposingly directed but nearly identically folded peripheral domains. FMN is positioned asymmetrically within the junctional site and is specifically bound to RNA through interactions with the isoalloxazine ring chromophore and direct and Mg^{2+}-mediated contacts with the phosphate moiety. Our structural data, complemented by binding and footprinting experiments, imply a largely pre-folded tertiary RNA architecture and FMN recognition mediated by conformational transitions within the junctional binding pocket. The inherent plasticity of the FMN-binding pocket and the availability of large openings make the riboswitch an attractive target for structure-based design of FMN-like antimicrobial compounds. Our studies also explain the effects of spontaneous and antibiotic-induced deregulatory mutations and provided molecular insights into FMN-based control of gene expression in normal and riboflavin-overproducing bacterial strains.

Riboswitches that target protein cofactors constitute the most abundant class of untranslated messenger RNA (mRNA) regions capable of direct sensing of cellular metabolites[8]. Recent three dimensional structures of thiamine pyrophosphate (TPP)[9–11] and S-adenosyl-L-methionine (SAM)[12,13] riboswitches provided the first insights into the molecular organization of cofactor-specific riboswitches. Nevertheless, additional structural studies are required to explain the principles of RNA folding and ligand recognition for larger riboswitches, such as those that target adocobalamin1[4] and FMN[4,5]. The determination of the FMN riboswitch structure could be especially interesting and timely, given the predicted complexity of its riboswitch fold, the abundance of this riboswitch in pathogenic species[7,8]

Correspondence and requests for materials should be addressed to A.S. (serganoa@mskcc.org) or D.J.P. (pateld@mskcc.org)..
*These authors contributed equally to this work.

Full Methods and any associated references are available in the online version of the paper at www.nature.com/nature.

Supplementary Information is linked to the online version of the paper at www.nature.com/nature.

Author Contributions L.H. crystallized the F. nucleatum FMN riboswitch and performed binding experiments, A.S. determined the structures and performed footprinting experiments, and A.S. and D.J.P. wrote the manuscript with the assistance of L.H. All authors discussed the results and commented on the manuscript.

Author Information The coordinates of the X-ray structures of the FMN riboswitch are deposited in the RCSB Protein Data Bank under the following accession numbers: bound to FMN, transcribed RNA, 3F2Q; bound to FMN, two-strand composition, 3F4E; bound to riboflavin, 3F4G; bound to roseoflavin, 3F4H; $[Ir(NH_3)_6]^{3+}$ -soaked, 3F2T; Cs^+-soaked 3F2X; Ba^{2+}-soaked, 3F2W; Mn^{2+}-soaked, 3F2Y; $[Co(NH_3)_6]^{3+}$ -soaked, 3F30. Reprints and permissions information is available at www.nature.com/reprints.

and its involvement in riboflavin overproduction in biotechnologically relevant bacterial strains[15].

Fusobacterium nucleatum plays a role in periodontal disease and other human infections and is considered one of the most pathogenic bacteria of the genus[16]. The intracellular concentration of FMN in *F. nucleatum* is apparently controlled by a transcription attenuation mechanism involving two riboswitches, positioned before the riboflavin synthetic genes of the ribHDE(B/A) operon and the candidate riboflavin transporter *impX* gene (Supplementary Fig. 1)[17].

We have determined the 2.95-Å structure of the FMN-bound 112-nucleotide *F. nucleatum impX* RFN element, which conforms well with the consensus sequence and the six-helical junctional secondary structure characteristic of this riboswitch family (Fig. 1a–c and Supplementary Fig. 2a, b). The structure features a complex FMN bound junctional region stapled together by two peripheral domains, P2–P6 and P3–P5. Each peripheral domain is formed by two interacting stem-loops, stabilized by two pairs of tertiary contacts involving loop–loop (L2–L6 and L3–L5) and loop–helix (L6–P2 and L3–P5) interactions (Fig. 1a and Supplementary Fig. 3a, b), resulting in an overall butterfly-like fold (Fig. 1c). Stems P1 and P4 radiate in opposite directions from the bottom part of the junction. Most unexpectedly, the peripheral domains show nearly identical conformations when superposed by ~180° rotation along the axis directed through the central region of the riboswitch (Fig. 1d). Though symmetry is not a characteristic feature of large RNAs, such local symmetry has also been identified in the ribosome[18]. Surprisingly, the pseudo-symmetrical FMN does not take advantage of the twofold symmetry between riboswitch elements, because its isoalloxazine ring and phosphate are oriented towards different riboswitch domains. The peripheral domains contain small RNA motifs[19,20], such as a T-loop[8,21,22] (Supplementary Fig. 3c), and show a striking resemblance to larger architectural modules found in 23S ribosomal RNA (rRNA)[19] (Supplementary Fig. 4). Despite this similarity, the domains serve as molecular staples to hold and shape the FMN binding pocket in the riboswitch, whereas in rRNA they form stable platforms for interactions with proteins and other rRNA segments[23].

Comparison of the loop–helix interactions uncovers a small difference that may contribute to gene expression regulation. In the P2–P6 domain, invariant G12 from the G12•(G93–C30) triple (Fig. 1e) replaces the corresponding A63 in the stable A-minor A63•(G41–C82) triple from the P3–P5 domain (Fig. 1f). To prevent a steric clash with the G93–C30 pair, the G12 base is moved out of the triple plane, thereby weakening both G12•(G93–C30) and G11•(G84–C31) triples. The lower stability of these adjacent triples could enhance the mobility of the J1-2 segment, highlighting its contribution to the coenzyme-sensitive switch governing gene regulation. In essence, the J1-2 segment participates in anti-terminator formation in the absence of FMN, whereas in the FMN-bound state it is locked up in the junction, thereby facilitating formation of the regulatory P1 helix.

In contrast to other multi-stem junctional riboswitches[9–11,13,24–27], the junctional region of the FMN riboswitch is not constructed on the basis of collinear stacking of adjacent helices, but instead is composed of several non-paired segments, which provide a smooth transition between adjacent helices (Fig. 1c and Supplementary Fig. 3d, e). Unlike coenzymes in other riboswitches[9–11,13], the oxidized FMN is positioned centrally inside the junctional region and is surrounded by all six RNA stems (Figs 1c and 2a). The planar isoalloxazine ring system intercalates between A48 and A85, thereby providing a continuous stacking alignment linking P6 and P3 helices. The uracil-like edge of the ring system forms specific Watson–Crick-like hydrogen bonds with the highly conserved A99 (Fig. 2b). The ribityl moiety of FMN uses only one of its four oxygens for hydrogen bonding, whereas phosphate

oxygens form additional hydrogen bonds with Watson–Crick edges of several conserved guanines. The interaction between the phosphate of FMN and RNA is also bridged by metal ion M1, assigned as Mg^{2+}, which directly coordinates the phosphate oxygen of FMN and the N7 position of G33, and forms several water-mediated contacts with neighbourikng nucleotides (Fig. 2c). In support of the structural data, the binding affinity of riboflavin, the FMN precursor, which lacks the phosphate and does not control gene expression, decreases by about 1,000-fold, compared with binding of FMN to both *F. nucleatum* and *Bacillus subtilis*[5] riboswitches (Fig. 2d and Supplementary Fig. 5). The additional removal of the ribityl moiety in lumiflavin reduces binding affinity to only a very small extent (Fig. 2d). In contrast to the FMN riboswitch, the *in-vitro*-selected RNA aptamer does not bind the phosphate moiety of FMN and uses the Hoogsteen edge of adenine for specific recognition of the ring system (Supplementary Fig. 6)[28].

The identity of metal M1 as Mg^{2+} has been confirmed by substitution with Mn^{2+}, a mimic of Mg^{2+} (Supplementary Fig. 7). Cs^{+} cations failed to replace M1 and were found in the P3 stem and next to the FMN ring system (Supplementary Fig. 8), where a Cs^{+} replaces a K^{+} (labelled M2, Fig. 2a) cation. The interactions between FMN and the riboswitch critically depend on the physiological concentration of Mg^{2+} (Fig. 2e and Supplementary Fig. 9a), and can be enhanced further by addition of 100 mM K^{+} (Supplementary Fig. 9b). Smaller and larger monovalent cations, such as Na^{+} and Cs^{+}, potentiate FMN binding to a lesser extent than K^{+} (Supplementary Fig. 9c). The identity of the divalent cation appears not to be crucial for FMN binding, because Mg^{2+} can be substituted by Ca^{2+}, as well as Ba^{2+} and Mn^{2+}, even in the absence of monovalent cations (Supplementary Figs 9a, b and 10). It is likely that cation M1contributes significantly to the metal dependence of the FMN binding, because the coenzyme binds the riboswitch equally well in the presence of cobalt hexamine, which can be accommodated with some adjustments in the M1 position (Supplementary Figs 9b and 11), whereas bulkier iridium hexamine, which does not fit into the M1position, reduces binding affinity about 15-fold (Supplementary Figs 9b and 12). Unlike the M1 site, the M2 position constitutes part of a larger cation-binding area, which extends towards G11 and FMN and which can accommodate all soaked metals, except Mn^{2+}. Though cations in this area stabilize the FMN-binding pocket, the weaker dependence of FMN binding on monovalent cations (Supplementary Fig. 9a, b) suggests a less critical role of the M2 site for FMN–riboswitch complex formation.

To gain further insights into the ligand discrimination by FMN riboswitches, we have determined crystal structures of the riboswitch in complex with riboflavin and roseoflavin[7] (Fig. 3a, b). In the riboflavin-bound structure, the P4 helix is shifted towards the ligand-binding pocket (Supplementary Fig. 13a) and several nucleotides that are close to the phosphate-binding cavity and the hydrophobic edge of the ring system become slightly re-positioned (Fig. 3a). The roseoflavin-bound structure adopts a conformation similar to the riboflavin-bound structure (Supplementary Fig. 13b), with additional spatial adjustments of U61 and G62 to accommodate the dimethylamino group that substitutes for a methyl on the hydrophobic edge of the isoalloxazine ring system (Fig. 3b). Such ligand dependent conformational changes have been described earlier only for the TPP riboswitch[11]. In contrast to similar recognition of the ring system, the ribityl moieties of all three FMN riboswitch ligands adopt slightly different conformations and exhibit somewhat different interactions with the RNA. As expected, no metal M1 was found in the two analogue complexes, given that analogues lack a phosphate group. The transcription of the mRNA that contains the FMN riboswitch was found to be inhibited *in vitro* by another coenzyme, flavin adenine dinucleotide (FAD)[4], used at a 17-fold higher concentration than FMN. Our structure-based modelling of a FAD-riboswitch complex supports the possibility of FAD-mediated control of the FMN riboswitch[4] because FAD can be accommodated within the binding pocket after minor conformational adjustments (Supplementary Fig. 14). The

observed plasticity of the ligand-binding pocket, together with the large openings next to the edges of the ring system (Fig. 3c) and the phosphate-binding site (Supplementary Fig. 15), makes the FMN riboswitch an attractive target for the structure based design of FMN-like antimicrobial compounds.

Because the bound FMN is enveloped by the RNA, the FMN riboswitch is anticipated to re-arrange its conformation on complex formation. To access these potential conformational changes, we have performed footprinting experiments using nucleases V1 (paired and stacked regions) and T2 (single-stranded regions) (Fig. 4a). Despite similar conformations of the peripheral domains, the P2–P6 domain is more accessible to both nucleases (Supplementary Fig. 16), and exhibits more pronounced FMN-induced changes (Fig. 4b) than its P3–P5 counterpart, implicative of a more rigid conformation for the P3–P5 domain. Nevertheless, the FMN-induced changes in the peripheral domains are not extensive and are consistent with a largely pre-formed conformation for these regions. The presence of V1 and the absence of T2 cleavages indicate that nucleotides of the junctional segments are most likely involved in stacking interactions in the unbound state. Most of these nucleotides, which are clustered around the phosphate (nucleotides 10, 29–33) and isoalloxazine ring system (nucleotides 46–50, 97–102) of FMN and are adjacent to the P1 helix (nucleotides 9, 104), become protected on FMN binding owing to the mobility restrictions and shielding by neighbouring RNA segments. Our structural and footprinting data, corroborated by the in-line probing results on the *B. subtilis* riboswitch[5] (Supplementary Fig. 17), suggest that the primary recognition event(s) may involve Mg^{2+}-mediated interaction of the FMN phosphate with RNA, coupled with intercalation and base-specific interactions involving the isoalloxazine ring system. These interactions should stabilize the J1-2 segment (G10–G12) and, in accordance with the strongest protections (Fig. 4a, b), bring the nuclease-accessible J6-1 segment (A99–G104) and the C8–G9 step close to each other. Such positioning provides partial stacking between the J6-1 segment (A99–G104) and the helix P1-forming strands, and facilitates formation of the non-canonical G10•G47 pair, the type I A-minor motif based G9•A104•(G33–C46) tetrad, the C8–G105 base pair, and other base pairs of the P1 helix (Fig. 4c).

Because riboflavin biosynthetic capability is lacking in higher animals, riboflavin is traditionally used for food and feed fortification. Riboflavin can be produced in bacterial strains selected as roseoflavin resistant mutants with deregulated riboflavin biosynthesis[15]. The FMN riboswitch structure (Supplementary Fig. 18) readily explains the effects of deregulated mutations[15,29]. Surprisingly, most of the mutations are concentrated in the peripheral domains, where they destabilize the helices or directly disrupt tertiary contacts. Mutations G32A/C and G62A found in the FMN-binding pocket disrupt the G62•(C83–G32) triple (Fig. 1f), which interacts with the Mg^{2+}-coordinated phosphate of FMN. Two other mutations, G105U and G108A, prevent formation and/or affect stability of the regulatory P1 helix.

Recent studies have demonstrated slow kinetics of association and dissociation for the FMN–riboswitch complex, supportive of a kinetically driven riboswitch mechanism[30]. These kinetic characteristics are consistent with the recognition principles identified in our three-dimensional structure. Indeed, riboswitch folding requires formation of multiple non-canonical and tertiary interactions and other conformational adjustments on FMN binding, which together may account for the slow association rate. Subsequent FMN release is likely to be slowed down due to envelopment of the ligand by the RNA. The propensity of other large riboswitches to function as kinetically driven genetic switches remains a challenging area for future exploration.

METHODS

RNA preparation and complex formation

The 112-nucleotide sensing domain of the *F. nucleatum* FMN riboswitch followed by a hammerhead ribozyme was cloned into the pUT7 vector[31] and transcribed in vitro using T7 RNA polymerase. The RNA was purified by denaturing polyacrylamide gel electrophoresis and anion-exchange chromatography. Alternatively, the riboswitch was formed by the annealing of two chemically synthesized RNAs (0.4 mM each), 59-GGAUCUUCGGGGCAGGGUGAAAUUCCCGACCGGUGGUAUAGUCCACGAAAGCUU and 59-GCUUUGAUUUGGUGAAAUUCCAAAACCGACAGUAGAGUCUGGAUGAGAGAAGAUUC, designed to engineer crystal contacts, in the presence of FMN or its analogues in the binding buffer at 37 °C for 30 min followed by incubation on ice. The 143-nucleotide sensing domain of the *B. subtilis* FMN riboswitch, the 220-nucleotide full-length *F. nucleatum* FMN riboswitch and the 172-nucleotide fragment of the *B. subtilis* lysine riboswitch[27] were transcribed and purified as above. Ligand concentrations were estimated spectrophotometrically using the extinction coefficients ε_{450}=12,500 $M^{-1}cm^{-1}$ for FMN, ε_{505}=31,000 $M^{-1}cm^{-1}$ for roseoflavin, and ε_{445}=12,500 M cm^{-1} for riboflavin and lumiflavin.

Crystallization and X-ray crystallography

Crystals were grown at 20 °C using hanging-drop vapour diffusion by mixing 1 ml complex with 1 ml reservoir solution. The FMN-bound complex produces crystals of the saturated yellow colour, characteristic for the oxidized form of FMN, under several conditions. The best crystals were obtained in the solution containing 0.1 M MES-sodium, pH 6.5, 100–200 mM $MgCl_2$ and 6–13% (w/v) PEG 4000 for 1–4 weeks. The crystals of the analogue-bound complexes grew in solution containing 0.1M Tris-HCl, pH 8.4, 200mM $MgCl_2$ and 6–10% (w/v) PEG 4000 for about 1 week. The FMN-bound native and heavy-atom-soaked crystals were grown using the transcribed RNA. Although the analogue-bound crystals could grow using the transcribed RNA, resolution of the crystals was improved with the annealed riboswitch. X-ray diffraction data were reduced using HKL2000 (HKL Research). The structure was determined using 3.0-Å MAD iridium data and autoSHARP[32]. The RNA model was built using TURBO-FRODO (http://www.afmb.univmrs.fr/-TURBO-) and refined with REFMAC[33]. The final 2.95-Å riboswitch model contained 109 nucleotides (nucleotides 54–56 were cleaved off during crystallization), one FMN molecule, two potassium and 14 magnesium cations. Mn^{2+}, Cs^{+}, Ba^{2+} and $[Co(NH_3)_6]^{3+}$ cations were positioned based on the anomalous electron density maps (Supplementary Figs 7, 8, 10 and 11). Mg^{2+} and K^{+} cations were modelled according to location of their mimics, coordination geometry and distances[34].

Fluorescence measurements

Fluorescent assays were performed based on intrinsic fluorescence of FMN and its analogues, which become quenched after specific interaction of the ligands with the riboswitch fragment. In all assays, intensity of fluorescence emission was measured at 530 nM with excitation at 450 nM. Each experiment was performed about two to four times at room temperature using a Tecan M1000 fluorimeter. For the binding affinity measurements, the fragments of the *F. nucleatum* and *B. subtilis* FMN riboswitches were titrated against 6×10^{-8} M FMN or 10^{-8} M analogs. RNA and ligands were premixed in 50 mM Tris-HCl, pH 7.4, 100 mM KCl and 2 mM $MgCl_2$ in the 96 half-area black flat plates for 10–60 min. The *B. subtilis* lysine riboswitch[27] was used as a negative control. After subtraction of the buffer fluorescence and normalization to the free ligand fluorescence, the data were fitted to equation (1):

$$F = 1 + (f - 1)\frac{(L_0 + R_0 + K_d) - \sqrt{(L_0 + R_0 + K_d)^2 - 4L_0R_0}}{2L_0} \quad (1)$$

where F is normalized fluorescence intensity, L_0 and R_0 are the concentrations of ligand and RNA, K_d is the apparent dissociation constant, and f is a residual fluorescence intensity at the saturated concentration of ligand, determined by plotting F versus R_0. For cation-dependence studies, the 112-nucleotide *F. nucleatum* FMN riboswitch was titrated against 6×10^{-8} M of FMN in 50 mM Tris-HCl, pH 7.4, supplemented with 2 mM different cations ($MgCl_2$, $MnCl_2$, $BaCl_2$, $CaCl_2$, $[Ir(NH_3)_6]Cl_3$ and $[Co(NH_3)_6]Cl_3$) in the presence and absence of 100 mM KCl or in the presence of other monovalent cations (NaCl or CsCl). Binding affinities were determined using equation (1). The cation concentration required for the FMN binding was estimated by titration of different cations against a mixture of RNA (2×10^{-7} M) and ligand (6×10^{-8} M) in 50 mM Tris-HCl, pH 7.4. After background subtraction of the fluorescent quenching at each point in the absence of RNA, data were fitted to the Hill equation (2),

$$\theta = [M]^n / (K_d + [M]^n) \quad (2)$$

where h is the normalized FMN-bound fraction, n is Hill coefficient, [M] is the concentration of cation and K_d is the apparent dissociation constant. As the parameters K_d and n covary, the cation binding was roughly estimated as the ion concentration $[M]_{1/2}=(K_d)^{1/n}$ at which approximately 50% of FMN was bound to RNA.

Footprinting studies

For footprinting experiments[35], the 112-nucleotide *F. nucleatum* riboswitch was radioactively labelled at the 5′ end by the kinase reaction. Samples (20 ml) of the radiolabelled RNA (100,000 c.p.m.) with a final RNA concentration 0.5 mM were preheated at 37 °C for 10 min in 50 mM Na- HEPES, pH 7.9, 50 mM KCl and 2 mM $MgCl_2$. Six-fold excess of FMN was added to the RNA and the mixtures were additionally incubated at 37 °C for 15 min. Cleavage reactions were performed with 0.003 U RNase V1 (Pierce) or 0.25 U RNase T2 (Sigma) at 37 °C for 10 min. Reactions were quenched by the addition of 80 ml cold buffer and were immediately extracted with phenol-chloroform and precipitated by ethanol. Radiolabelled pellets were dissolved and analysed by polyacrylamide gel electrophoresis.

Supplementary Material

Refer to Web version on PubMed Central for supplementary material.

Acknowledgments

We thank the personnel of beamline X29 at the Brookhaven National Laboratory and beamline 24-ID-C at the Advanced Photon Source, Argonne National Laboratory, funded by the US Department of Energy. We thank L. Jaeger (University of California, Santa Barbara) for discussions and O. Ouerfelli (Memorial Sloan-Kettering Cancer Center, New York) for the synthesis of iridium hexamine. D.J.P. was supported by funds from the National Institutes of Health.

References

1. Nudler E, Mironov AS. The riboswitch control of bacterial metabolism. Trends Biochem. Sci. 2004; 29:11–17. [PubMed: 14729327]
2. Serganov A, Patel DJ. Ribozymes, riboswitches and beyond: regulation of gene expression without proteins. Nat. Rev. Genet. 2007; 8:776–790. [PubMed: 17846637]

3. Winkler WC, Breaker RR. Regulation of bacterial gene expression by riboswitches. Annu. Rev. Microbiol. 2005; 59:487–517. [PubMed: 16153177]
4. Mironov AS, et al. Sensing small molecules by nascent RNA: a mechanism to control transcription in bacteria. Cell. 2002; 111:747–756. [PubMed: 12464185]
5. Winkler WC, Cohen-Chalamish S, Breaker RR. An mRNA structure that controls gene expression by binding FMN. Proc. Natl. Acad. Sci. U S A. 2002; 99:15908–15913. [PubMed: 12456892]
6. Gelfand MS, Mironov AA, Jomantas J, Kozlov YI, Perumov DA. A conserved RNA structure element involved in the regulation of bacterial riboflavin synthesis genes. Trends Genet. 1999; 15:439–442. [PubMed: 10529804]
7. Blount KF, Breaker RR. Riboswitches as antibacterial drug targets. Nat. Biotechnol. 2006; 24:1558–1564. [PubMed: 17160062]
8. Barrick JE, Breaker RR. The distributions, mechanisms, and structures of metabolite-binding riboswitches. Genome Biol. 2007; 8:R239. [PubMed: 17997835]
9. Serganov A, Polonskaia A, Phan AT, Breaker RR, Patel DJ. Structural basis for gene regulation by a thiamine pyrophosphate-sensing riboswitch. Nature. 2006; 441:1167–1171. [PubMed: 16728979]
10. Thore S, Leibundgut M, Ban N. Structure of the eukaryotic thiamine pyrophosphate riboswitch with its regulatory ligand. Science. 2006; 312:1208–1211. [PubMed: 16675665]
11. Edwards TE, Ferre-D'Amare AR. Crystal structures of the thi-box riboswitch bound to thiamine pyrophosphate analogs reveal adaptive RNA-small molecule recognition. Structure. 2006; 14:1459–1468. [PubMed: 16962976]
12. Gilbert SD, Rambo RP, Van Tyne D, Batey RT. Structure of the SAM-II riboswitch bound to S-adenosylmethionine. Nat. Struct. Mol. Biol. 2008; 15:177–182. [PubMed: 18204466]
13. Montange RK, Batey RT. Structure of the S-adenosylmethionine riboswitch regulatory mRNA element. Nature. 2006; 441:1172–1175. [PubMed: 16810258]
14. Nahvi A, et al. Genetic control by a metabolite binding mRNA. Chem. Biol. 2002; 9:1043–1049. [PubMed: 12323379]
15. Burgess CM, Smid EJ, Rutten G, van Sinderen D. A general method for selection of riboflavin-overproducing food grade micro-organisms. Microb. Cell. Fact. 2006; 5:24. [PubMed: 16848883]
16. Kapatral V, et al. Genome sequence and analysis of the oral bacterium Fusobacterium nucleatum strain ATCC 25586. J. Bacteriol. 2002; 184:2005–2018. [PubMed: 11889109]
17. Vitreschak AG, Rodionov DA, Mironov AA, Gelfand MS. Regulation of riboflavin biosynthesis and transport genes in bacteria by transcriptional and translational attenuation. Nucleic Acids Res. 2002; 30:3141–3151. [PubMed: 12136096]
18. Agmon I, Bashan A, Zarivach R, Yonath A. Symmetry at the active site of the ribosome: structural and functional implications. Biol. Chem. 2005; 386:833–844. [PubMed: 16164408]
19. Jaeger L, Verzemnieks EJ, Geary C. The UA_handle: a versatile submotif in stable RNA architectures. Nucleic Acids Res. 2008
20. Lescoute A, Westhof E. The interaction networks of structured RNAs. Nucleic Acids Res. 2006; 34:6587–6604. [PubMed: 17135184]
21. Krasilnikov AS, Mondragon A. On the occurrence of the T-loop RNA folding motif in large RNA molecules. RNA. 2008; 9:640–643. [PubMed: 12756321]
22. Nagaswamy U, Fox GE. Frequent occurrence of the T-loop RNA folding motif in ribosomal RNAs. RNA. 2002; 8:1112–1119. [PubMed: 12358430]
23. Selmer M, et al. Structure of the 70S ribosome complexed with mRNA and tRNA. Science. 2006; 313:1935–1942. [PubMed: 16959973]
24. Batey RT, Gilbert SD, Montange RK. Structure of a natural guanine-responsive riboswitch complexed with the metabolite hypoxanthine. Nature. 2004; 432:411–415. [PubMed: 15549109]
25. Serganov A, et al. Structural basis for discriminative regulation of gene expression by adenine- and guanine-sensing mRNAs. Chem. Biol. 2004; 11:1729–1741. [PubMed: 15610857]
26. Garst AD, Heroux A, Rambo RP, Batey RT. Crystal structure of the lysine riboswitch regulatory mRNA element. J. Biol. Chem. 2008; 283:22347–22351. [PubMed: 18593706]
27. Serganov A, Huang L, Patel DJ. Structural insights into amino acid binding and gene control by a lysine riboswitch. Nature. 2008; 455:1263–1267. [PubMed: 18784651]

28. Fan P, Suri AK, Fiala R, Live D, Patel DJ. Molecular recognition in the FMN-RNA aptamer complex. J. Mol. Biol. 1996; 258:480–500. [PubMed: 8642604]

29. Burgess C, O'Connell-Motherway M, Sybesma W, Hugenholtz J, van Sinderen D. Riboflavin production in *Lactococcus lactis*: potential for in situ production of vitamin-enriched foods. Appl. Environ. Microbiol. 2004; 70:5769–5777. [PubMed: 15466513]

30. Wickiser JK, Winkler WC, Breaker R, Crothers DM. The speed of RNA transcription and metabolite binding kinetics operate an FMN riboswitch. Mol. Cell. 2005; 18:49–60. [PubMed: 15808508]

31. Serganov A, et al. Ribosomal protein S15 from Thermus thermophilus: cloning, sequencing, overexpression of the gene and RNA-binding properties of the protein. Eur. J. Biochem. 1997; 246:291–300. [PubMed: 9208917]

32. de La Fortelle, E.; Bricogne, G. Methods in Enzymology. Academic Press; New York: 1997. p. 472-494.

33. Murshudov GN, Vagin AA, Dodson EJ. Refinement of macromolecular structures by the maximum-likelihood method. Acta Crystallogr. D Biol. Crystallogr. 1997; 53:240–255. [PubMed: 15299926]

34. Feig, AL.; Uhlenbeck, OC. The RNA World. Second Edition. Gesteland, RF.; Cech, TR.; Atkins, JF., editors. Cold Spring Harbor Laboratory Press; Cold Spring Harbor: 1999. p. 287-319.

35. Serganov A, Polonskaia A, Ehresmann B, Ehresmann C, Patel DJ. Ribosomal protein S15 represses its own translation via adaptation of an rRNA-like fold within its mRNA. EMBO J. 2003; 8:1898–1908. [PubMed: 12682022]

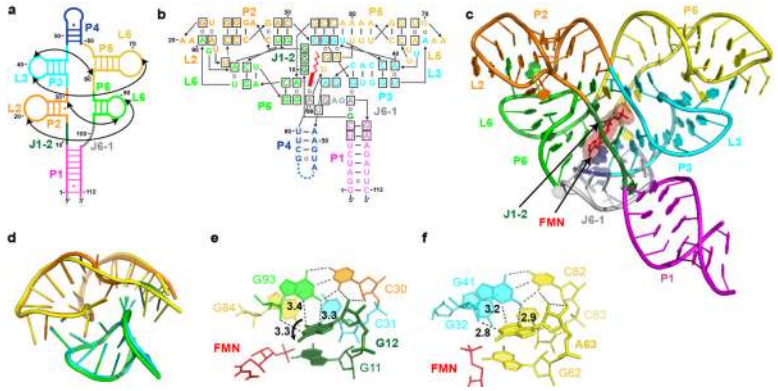

Figure 1. Overall structure and tertiary interactions of the FMN-bound *F. nucleatum* riboswitch

a, Homology-based schematic of the FMN riboswitch with key long-range interactions indicated by arrows. RNA segments are depicted in colours used for subsequent figures. **b**, Schematic of the riboswitch fold observed in the crystal structure of the complex. The bound FMN is in red. Key stacking interactions involving FMN are shown as blue dashed lines. Nucleotides that are more than 95% conserved among 183 FMN riboswitches are boxed. **c**, Overall riboswitch structure in a ribbon representation. **d**, Superposition of the P2–P6 (nucleotides 10–32 and 85–98) and P3–P5 domains (nucleotides 62–84 and 33–46). The root mean square deviation is 1.8 Å. **e**, **f**, Distinct alignments of nucleotide triples in the P2–P6 (e) and P3–P5 (f) domains. Dashed lines depict putative hydrogen bonds. Distances are in ångstroms.

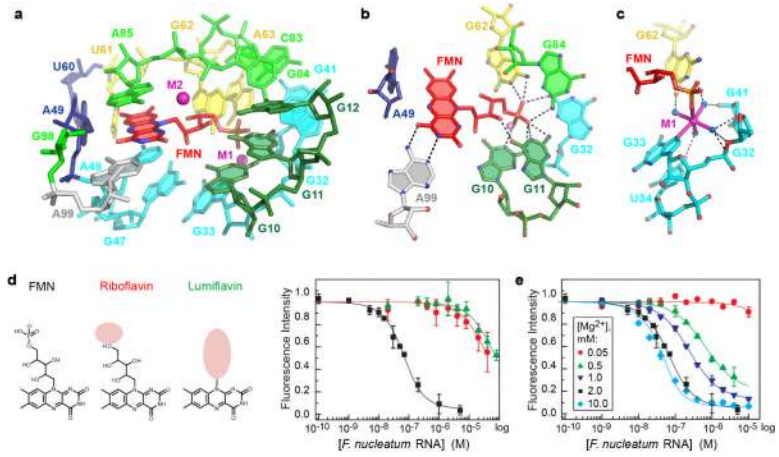

Figure 2. Recognition of FMN by its riboswitch

a, A view of the junction with bound FMN. Magenta spheres depict cations in proximity to FMN. **b**, Details of riboswitch–FMN interactions. Hydrogen bond distances are shown with dashed lines. **c**, FMN–riboswitch interactions mediated by M1, assigned to an Mg^{2+} cation. Magenta sticks depict coordination bonds. Mg^{2+}-coordinated water molecules (blue spheres) are positioned on the basis of direct coordination bonds with phosphate and G33. **d**, Chemical structures (left panel) and fluorescent binding assay (right panel) of FMN and its analogues with the 112-nucleotide *F. nucleatum* riboswitch conducted in 2 mM $MgCl_2$ and 100 mM KCl. The dissociation constants (micromolar, mean±s.d.) are: FMN, 0.0375±0.0031; riboflavin, ~39.8; lumiflavin, ~59.0. e, Interaction of FMN with *F. nucleatum* riboswitch in 100 mM KCl as a function of variable Mg^{2+} concentration. The dissociation constants (nanomolar, mean±s.d.) are: 0.5 mM $MgCl_2$, 406.0±52.7; 1.0 mM $MgCl_2$, 211.7±2.1; 10.0 mM $MgCl_2$, 10.9±2.4.

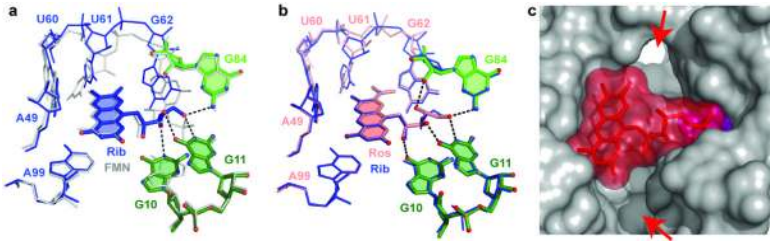

Figure 3. Interactions of FMN analogues with the riboswitch

a, All-atom superposition of the ligand-binding pocket for riboflavin-bound (blue and green) and FMN-bound (grey) riboswitches. Nucleotides in green are positioned within hydrogen-bond distances of the ribityl moiety of riboflavin. **b**, Superposition of riboflavin-bound (blue) and roseoflavin-bound (pink and green) riboswitches, depicted as in **a**. **c**, Surface view inside of the FMN-bound riboswitch with large openings shown with red arrows.

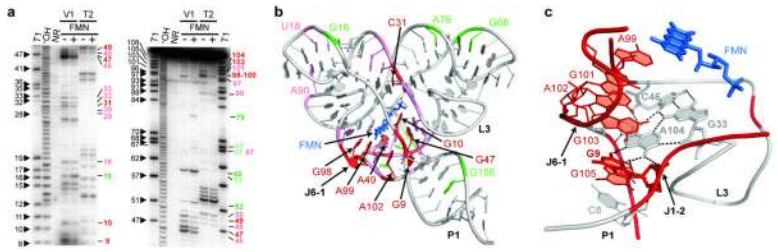

Figure 4. Probing the FMN riboswitch tertiary structure

a, Probing of 5′ ^{32}P-labelled 112-nucleotide RNA (0.5 mM) by V1 and T2 nucleases in the absence and presence of six-fold excess of FMN. T1 and $^{-}$OH designate RNase T1 and alkaline ladders, respectively. NR, no reaction. Weak and strong FMN-induced cleavage protections are shown in light and dark red, whereas weak and strong cleavage enhancements are shown in light and dark green. **b**, Projections of the nuclease cleavage reductions (light and dark red) and enhancement (green) on the riboswitch structure. **c**, Nucleotides potentially facilitating formation of the regulatory P1 helix. Hydrogen bonds in the G9•A104•(G33–C46) tetrad are indicted. FMN-induced cleavage reductions in the in-line probing assay[5] are in red.